Journal of Catalysis **210,** 218–228 (2002)
doi:10.1006/jcat.2002.3656

Modification of the Acid Properties of Silica–Zirconia Aerogels by *in Situ* and *ex Situ* Sulfation

Daniel J. Rosenberg,* F. Coloma,† and James A. Anderson*,[1]

*Surface Chemistry and Catalysis Group, Division of Physical and Inorganic Chemistry, University of Dundee, Dundee DD1 4HN, Scotland, United Kingdom; and †Departamento Química Inorgánica, Universidad de Alicante, Apdo. 99, 03080 Alicante, Spain

Received February 18, 2002; revised April 23, 2002; accepted April 23, 2002

Sulfated silica–zirconia mixed oxides containing 33 mol% Zr were prepared by sol-gel routes with the sulfate/zirconia molar ratio varying between 0.2 : 1 and 0.3 : 1. The influence of the added sulfate introduced by both *in situ* and *ex situ* methods on the bulk and surface properties was examined and in particular the role of sulfate in modifying the acid site density. Both silica and sulfate (*in situ*) were well distributed throughout the solid, thus delaying the onset of crystallization of zirconia phases. *Ex situ* sulfuric acid treatment resulted in extraction of a proportion of the zirconia to the surface to form small amorphous zirconia clusters, thus increasing Lewis acidity at the expense of Brønsted acid sites. As the sulfate concentration was increased beyond an estimated 2.82 SO_4^{2-} per square nanometer of exposed zirconia, this Lewis acidity was replaced by Brønsted acid sites. The maximum number of Brønsted acid sites which could be created by sulfate treatment was only marginally greater than the site density on a nonsulfated sample, although the site strength was much greater for the former. The distribution of components and in particular the role played by segregated, amorphous zirconia at the surface is discussed in terms of the modification of both Lewis and Brønsted acid sites.

INTRODUCTION

Acid catalysts are widely used in oil-refining processes to give improved fuels and feedstock hydrocarbons for the solvent, polymer, pharmaceutical, additives, and detergents industries. Reactions catalyzed by acid catalysts include isomerizations, alkylations, catalytic reforming of alkanes, cracking, and those involving oxygenated hydrocarbons. Solid acid catalysts are also being introduced into highly selective chemical and fine-chemical synthesis. The nature of the active site in solid acid catalysts is defined by the presence of protons, generating Brønsted acidity, and by coordinately unsaturated cationic centers that give Lewis acid sites (1). Mixed oxides often show different forms of acidity from the individual component oxides with the most widely accepted model for the generation of acid sites on mixed oxides involving charge imbalance imposed upon the minor component oxide by the imposition of the bond matrix of the major component (2, 3), where the minor component oxide metal retains its coordination. Recent alternatives to this model still rely on charge imbalance resulting from heteroatom linkages for the creation of acid centers (4, 5) while models based on electrostatic potential differences of a cationic center in the two different matrices (6) fail to account for the acid sites generated in 50 mol% samples. The acidity shown by supported oxides is incompatible with models that rely on the extent of component mixing and the formation of heterolinkages.

One method of obtaining homogeneously mixed oxides containing two or more components involves sol-gel methods. The use of sol-gel chemistry to prepare mixed oxides introduces a high degree of flexibility because their final properties can be deliberately influenced by manipulation of their preparation parameters. Millar *et al.* and the authors (7–11) have used this approach to prepare silica–zirconia aerogels where the influence of the degree of mixing and the Si/Zr ratio on the density and strength of generated acid groups have been determined.

An alternative method of modifying the acid properties of a solid oxide is by use of dopant ions; sulfate is the mostly widely used. The enhanced surface acidity and possible superacid catalytic properties resulting from sulfate addition is most widely recognized in the case of neat zirconia (12–14). However, the surface acid properties of transition metal promoted and alumina-containing sulfated zirconias have been reported (15, 16) as has the influence of sulfate on the acidic properties of silica–titania (17) and silica–zirconia (18) mixed oxides. Sulfation is often achieved via a wet impregnation technique whereby the mixed oxide is contacted with an aqueous solution of sulfuric acid. However, this method has been reported to induce segregation at the surface of both silica–zirconia (19) and silica–titania (17) mixed oxides as a result of hydrolysis of the Si–O–M bonds leading to extraction of the M cation. This results in amorphous sulfated zirconia or titania being deposited on silica. Sulfation may also influence the onset temperature of crystalization of zirconia (20). When a mixed oxide is sulfated in such a manner, the sulfur-containing species are

[1] To whom correspondence should be addressed. E-mail: j.a.Anderson@dundee.ac.uk.

0021-9517/02 $35.00

thought to be exclusively associated with the nonsilica component of the mixed oxide (21). This means that a sulfated silica–zirconia mixed oxide may be thought of as sulfated zirconia dispersed within a silica lattice.

It is known that in the case of sulfated zirconia materials, three preparative parameters are crucial in determining the overall acid properties of the samples (12). These are the temperature of calcination of the nonsulfated zirconia precursor, the surface sulfate concentrations, and the *in situ* thermal activation of the sulfated zirconia (12). In the current study, the calcination temperature and *in situ* pretreatment temperatures have been fixed to limit the number of preparation variables, and only the methods of sulfate incorporation and sulfate loadings have been varied. Details are presented for a series of sulfated silica–zirconia aerogels, prepared by both *in situ* and *ex situ* procedures for samples where the Si/Zr ratio was held constant while the SO_4^{2-} : Zr ratio was varied from 0.2 : 1 to 0.3 : 1.

EXPERIMENTAL

Sample Preparation

A sulfate-free and a number of sulfated 33 mol% zirconia–silica mixed oxides were prepared by modifying the method described by Yoldas (22). Tetraethyl orthosilicate, TEOS (Silibond, 90 wt%), was combined with water, propanol (Aldrich) as a solvent, and nitric acid (Aldrich) used as a hydrolysis catalyst. These were combined in overall ratios of 1 : 1.2 : 1.5 : 0.2, respectively. The reagents were stirred under nitrogen for 2 h prehydrolysis time, after which zirconium isopropoxide (Aldrich, 70 wt%) diluted 10 : 1 in propanol was added (23) such that the ratio of Si^{4+} to Zr^{4+} was 2 : 1. After an additional hour the final amount of hydrolysis water was added dropwise, and the final water to metal cation ratio was 2.6 : 1. All samples gelled within approximately 3 days. Propanol was then exchanged for ethyl acetate via Soxhlet extraction for 5 h, and the ethyl acetate was subsequently removed using supercritical drying. Initially the sample was left for 12 h in supercritical CO_2 followed by a 30 min period of flushing every 2 h until no further ethyl acetate was detected in the effluent (typically after five flushes). Samples were then transferred to a tube furnace and calcined in flowing air at 873 K for 6 h. *In situ* sulfated samples were prepared in a similar manner but using sulfuric acid in varying amounts as the hydrolysis catalyst, with the H^+ concentration held constant by use of nitric acid. *Ex situ* sulfation involved addition of appropriate amounts of 0.01 M sulfuric acid to a precalcined aerogel followed by further calcination at 873 K. Samples were labeled as SiZr (*x*-*y*) where *x* refers to the mole ratio of sulfate relative to 1 zirconium in the preparation method and *y* appears as *in* or *ex* depending on whether sulfate addition was by *in situ* or *ex situ* method. For comparison purposes, samples of zirconia and sulfated zirconia were also prepared. This was achieved via precipitation from zirconium isopropoxide (Aldrich, 70 wt%). The same $H^+ : H_2O : Zr^{4+}$: propanol ratios were employed as used during the preparation of the mixed oxides. A sulfated zirconia, prepared by the use of sulfuric acid as hydrolysis catalyst, was prepared for comparative purposes and had a nominal S : Zr ratio of 0.30 : 1.

A sample where segregation of components was induced by thermal treatment was prepared by calcination at 1373 K of the nonsulfated SiZr (0) for 6 h.

Characterization

BET surface areas were measured using a multipoint Coulter SA 3100 instrument with data collected over the P/P_0 range of 0.02–0.2. Adsorption of N_2 at 77 K was carried out after outgassing the samples at 573 K. BJH pore distributions were determined using 45 data points over a full adsorption–desorption isotherm.

Surface acid densities were estimated using pyridine adsorption monitored by combined thermogravimetric and IR spectroscopic techniques (11). Thermogravimetric analyses were carried out using a PC-controlled microbalance attached to a conventional vacuum line fitted with rotary and diffusion pumps. Approximately 100 mg of sample as a fragmented disc (prepared as per IR experiments, described in the following) was outgassed for 2 h at 573 K, then exposed to 1 Torr pyridine and cooled to 373 K. An additional 0.5 Torr of pyridine was introduced and the system was allowed to reach equilibrium over 30 min. After this period, the sample was heated under vacuum to 423 K for 2 h, then at 473 K for 2 h while the mass was monitored continually at 3-s intervals throughout the experiment. The IR experiments were carried out in identical fashion using ca. 80 mg of sample pressed into a 2.5-cm diameter disc at 0.10 tons cm^{-2}. Spectra were recorded after the initial evacuation of the sample at 573 K and again following exposure to pyridine and outgassing at 423 and 473 K.

The mass of pyridine remaining adsorbed on the sample at the two adsorption temperatures, in combination with the integrated areas underneath the bands due to the 19b ring vibrations of pyridine adsorbed at Lewis and Brønsted sites (ca. 1450 and 1540 cm^{-1}, respectively) at the corresponding temperatures allowed calculation of the Brønsted and Lewis absorption coefficients. The number of Lewis and Brønsted sites could be calculated by fitting these data to the equation

$$n_T = A_L \times C_d/(\varepsilon_L \times m) + A_B \times C_d/(\varepsilon_B \times m),$$

where n_T is the total number of micromoles of pyridine per gram sample adsorbed at each temperature, A is the integrated absorbance (cm^{-1}) of IR bands due to pyridine on each site, C_d is the cross-sectional area (cm^2) of the pressed disc, ε is the absorption coefficient (cm μmole^{-1}) for pyridine at each site, and m is the mass (g) of the pressed disc.

Combined IR–gravimetric experiments were conducted between three and five times for each sample to ensure that the values obtained were reliable.

Sulfur contents were determined using a Leco CHNS-932 determinator. Samples were weighed within a silver capsule and then the encapsulated sample was dropped into a furnace when the components were combusted in an oxygen excess environment. The sulfur content measured as SO_2 was then determined by IR absorption.

X-ray photoelectron spectra were obtained using a VG Microtech Multilab electron spectrometer using the Mg $K\alpha$ radiation (1253.6 eV) from a twin anode in the constant energy analyzer mode with a pass energy of 50 eV. The pressure in the analysis chamber was maintained at 5×10^{-10} m bar. The binding energy and Auger kinetic energy scale were set by assigning a value of 284.6 eV to the C 1 s transition. The accuracy of the binding energy and Auger kinetic energy values were 0.2 and 0.3 eV, respectively.

59.6-MHz ^{29}Si MAS NMR spectra of the samples were obtained using a Chemagnetics CMX300 LITE multinuclear FT spectrometer. Powdered samples contained within 7.5 mm o.d. zirconia "pencil" rotors were spun at 4 kHz using compressed air. Instrument calibration was performed using 3(trimethylsilyl) 1-propanesulfonic acid sodium salt. Longitudinal (spin lattice) relaxation times (T_1) were obtained by using the saturation recovery pulse sequence, $[(\pi/2)_x]_{100}$–τ–$(\pi/2)_x$, where τ was varied from 0.1 to 600 s. T_1 was calculated using the relationship, $M = M_0(1 - \exp(-\tau/T_1))$, where M and M_0 represent intensity at recovery time τ and maximum intensity, respectively.

RESULTS

All samples prepared by the current methods gave gel times of around 3 days, somewhat longer than those achieved using previous preparation methods (11) but one which gave a higher degree of reproducibility among different batches. All SiZr samples other than the sample treated at 1373 K were X-ray amorphous. The high-temperature-treated sample gave peaks at 30, 34.5, and 50°, 2ϑ (Cu $K\alpha$ radiation), which correspond to values expected for tetragonal zirconia. These peaks were also apparent in the sample of sulfated zirconia. Table 1 includes some of the physical characteristics of the samples. The xerogels consistently showed very low BET areas of ca. 2–3 $m^2\ g^{-1}$, which contrasted significantly with the corresponding aerogels, which gave values in the 200–320 $m^2\ g^{-1}$ range. Because the method used for the xerogel preparation is a modified procedure for the preparation of glasses (22), this is not unexpected. The removal of solvent by supercritical drying led to formation of samples with suitably high surface areas with the improved preparation method adapted here, giving a marginally higher surface area (317 $m^2\ g^{-1}$) than the value reported (283 $m^2\ g^{-1}$) for the 33 mol% Zr sample prepared by our previous method (11). Sulfation of the aerogel followed by further calcination led to surface area loss of around 30% (Table 1). Partial replacement of nitric acid by sulfuric acid as hydrolysis catalyst had a significant effect of the surface area of the respective aerogel with a loss of up to 32%, although increasing the amount of sulfate actually led to a partial recovery of this lost surface area (Table 1). Previous studies have highlighted the fact that the nature of the hydrolysis catalyst between different acid types has a significant effect on the structural properties (and thus the resultant BET area) of silica–zirconia sol-gel-derived oxides (19, 24). The decreased area caused by replacement of nitric acid with sulfuric acid was also reflected in the measured values of pore volume (Table 1).

TABLE 1

Physical Characteristics of the Samples

Sample	BET[a] ($m^2\ g^{-1}$)	BET[b] ($m^2\ g^{-1}$)	Pore volume ($cm^3\ g^{-1}$)	Nominal sulfur content (wt%)	Measured sulfur content (wt%)	T_1 (s)
SiZr (0)	2.5	317	0.99	0	0	30.2
Segregated	—	16.7	0.09	—	—	96.4
SiZr (0.2-*in*)	—	213	0.58	2.44	1.54	40.6
SiZr (0.25-*in*)	3.0	235	0.77	3.00	2.13	40.3
SiZr (0.3-*in*)	—	257	0.75	3.56	3.00	42.3
SiZr (0.2-*ex*)	—	230	0.87	2.44	1.07	45.3
SiZr (0.25-*ex*)	—	212	0.82	3.00	1.84	44.2
SiZr (0.3-*ex*)	—	208	0.87	3.56	1.84	43.1
ZrO_2 (sulfated)	—	186	—	—	—	—

[a] Xerogel (samples calcined without prior supercritical drying in CO_2).
[b] Aerogel.

Unlike the use of nitric acid, where complete decomposition occurred during calcination and no nitrogen could be detected by elemental analysis, the use of sulfuric acid as hydrolysis catalyst (*in situ* samples) led to the formation of samples where a significant proportion of the sulfur was retained (Table 1). The relative amount of sulfur retained was always greater for the *in situ* than the corresponding *ex situ* prepared samples, possibly reflecting sulfur retained in the bulk of the material for the former. The presence of sulfur-containing species and/or modifications to the resultant mixed oxide as a result of the use of sulfuric acid in place of nitric acid was also reflected in the measured values of the ^{29}Si spin-lattice relaxation times (T_1) for the samples (Table 1). The incorporation of 33 mol% Zr reduced the T_1 value to 30.2 s from a value of ca. 120 s which is generally found for pure silica materials produced by similar methods (10). A sample of SiZr (0) which was calcined at 1373 K to induce crystallisation and thus segregation of the component oxides gave a T_1 value of 96.4 s. The sulfur-containing samples (*in situ*) all gave values around 40 s with no apparent dependence of the specific sulfur content on the measured spin-lattice relaxation time.

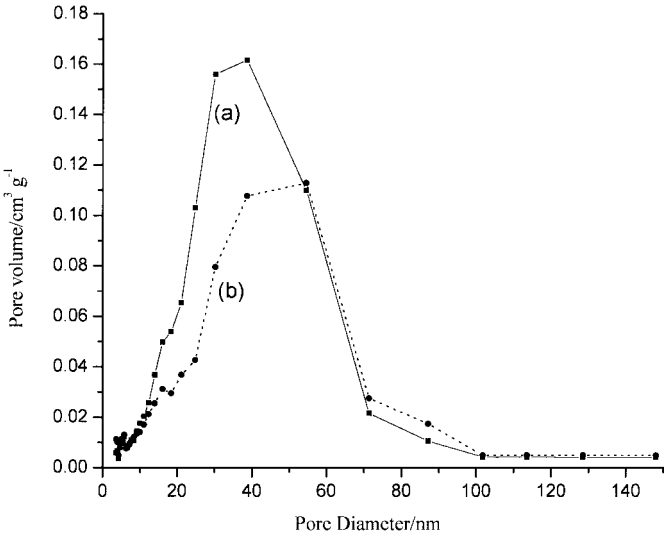

FIG. 1. Pore size distributions for (a) SiZr (0) (solid line representing the sulfate-free sample) and (b) SiZr (0.25) (dotted line representing a sulfated silica–zirconia).

Figure 1 shows the pore distribution profiles for a sulfate-containing and sulfate-free silica–zirconia mixed oxide. The sulfate-containing samples gave very similar profiles, giving three maxima at ca. 15, 45, and 90 nm, with by far the greatest volume held in pores of between 25 and 65 nm (Fig. 1, curve b). The sulfate-free sample also gave maxima at ca. 15 and 90 nm, but the mode was at ca. 35 nm and a much greater number of mesopores in the 25–65 nm range were present (Fig. 1, curve a).

The influence of hydrothermal treatment on the samples was analyzed by calcining, at 873 K (6 h) in a flow of air saturated with water vapor at 298 K, a sample that had previously been calcined in dry air at 873 K and a sample taken directly after supercritical drying. Direct hydrothermal calcination of the precursor gave a sample with BET area of 342 m^2 g^{-1} while hydrothermal treatment of the already calcined sample gave a BET area of 335 m^2 g^{-1}. Although hydrothermal treatments in both cases gave marginal improvements in total surface area, no obvious modifications to the pore distribution were detected.

Pyridine adsorbed on all the sulfate-free mixed oxides gave absorption bands indicative of the presence of both Lewis (1450 cm^{-1}) and Brønsted (1540 cm^{-1}) forms of acidity, unlike the component single oxides which do not generally exhibit the latter form of acidity. Additionally, a band at 1460 cm^{-1} which was present as a very weak feature in 9 mol% Zr–Si mixed oxide (9) was much more prevalent here, although it was always less intense than the 1450 and 1540 cm^{-1} maxima. The origin of this additional feature has been discussed for amorphous silica–alumina mixed oxides and zeolite samples (25). Should the origin of this band be a product of decomposition of pyridine, then this would have implications for the site densities measured by the combined IR–gravimetric techniques. All features were also observed for the sulfate-containing samples although the relative band intensities varied from sample to sample.

An indication of the relative total acidity (both Lewis and Brønsted forms) was obtained by measuring the total mass retained by the sample after removal of physisorbed and weakly bound pyridine by evacuation at 423 and 473 K. The mass of pyridine retained at both temperatures (Table 2) was less than reported for the previously prepared 33 mol% SiZr samples (11) when compared per unit surface area; however, both retained ca. 200 μmol g^{-1} after evacuation at 423 K. When acid densities were compared on a per mass basis, the *in situ* addition of sulfate had little effect on the amount of pyridine retained by the samples at both temperatures compared to the sulfate-free sample (Table 2, column 2); however, when compared on a per unit surface area basis (Table 2, column 3), it is clear that the presence of sulfate increased the acid site density of the mixed oxide. Increasing the S : Zr ratio increased the number of acid sites

TABLE 2

IR and Gravimetric Data for Pyridine Adsorption[a]

Sample	Conc[b]	Conc[c]	ε_{1540}[d]	ε_{1450}[d]	$n_{\text{Brønsted}}$[e]	n_{Lewis}[e]
SiZr (0)	198 (111)	0.625 (0.352)	0.53	1.78	0.217 (0.096)	0.161 (0.116)
SiZr (0.2-*in*)	169 (98)	0.794 (0.462)	0.77	2.08	0.279 (0.135)	0.202 (0.143)
SiZr (0.25-*in*)	179 (106)	0.762 (0.450)	0.66	1.74	0.253 (0.129)	0.204 (0.141)
SiZr (0.3-*in*)	199 (118)	0.773 (0.458)	0.64	1.98	0.274 (0.144)	0.191 (0.131)
SiZr (0.2-*ex*)	185 (120)	0.804 (0.522)	1.66	1.00	0.088 (0.049)	0.395 (0.266)
SiZr (0.25-*ex*)	174 (115)	0.820 (0.544)	1.18	1.11	0.121 (0.069)	0.374 (0.258)
SiZr (0.3-*ex*)	148 (91)	0.711 (0.437)	0.7	1.57	0.239 (0.133)	0.191 (0.134)

[a] Based on mass retained after evacuation of pyridine at 423 K (473 K).
[b] μmoles of pyridine per gram of sample.
[c] μmoles of pyridine per square meter of sample.
[d] IR absorption coefficient (cm μmol^{-1}).
[e] N^0 of acid sites per square nanometer (i.e., N^0 of pyridine molecules retained per square nanometer after evacuation at 423 K (473 K)).

per unit sample mass (Table 2, column 2); however, no clear tendency was apparent when samples were compared on a per unit area basis (Table 2, column 3). Sulfate addition by *ex situ* means had a more significant effect on the density of acid sites created. In addition to greater values than those for the sulfur-free sample, the SiZr (0.2-*ex*) and SiZr (0.25-*ex*) samples also displayed greater acid site densities than the *in situ* samples, although again, no clear tendency with respect to sulfur concentration was observed.

By combining IR and gravimetric measurements, absorption coefficients could be calculated for both forms of adsorbed species (Table 2). These were of a similar magnitude for both the pyridinium ion (0.53 to 1.66 cm μmol^{-1} at 1540 cm^{-1}) and Lewis-bound pyridine(1.00 to 2.08 cm μmol^{-1} at 1450 cm^{-1}). The absorption coefficients allowed calculation of the surface densities of both types of acid site as detected by pyridine (Table 2). Surface densities as determined by amount of adsorbate retained at 423 K were lower for the sulfate-free sample employed here than for an equivalent 33 mol% sample reported previously (11), again emphasizing the sensitivity of acid site formation to the exact nature of the prepared mixed oxide. The addition of sulfate (*in situ*) increased the density of both Brønsted and Lewis acid sites (Fig. 2 and Table 2, columns 6 and 7) relative to the sulfate-free sample. However, the addition of sulfate via this method did not, apparently, affect the proportion of pyridine retained after desorption at the higher evacuation temperature. The *ex situ* addition of sulfate gave more surprising results. The SiZr (0.3-*ex*) had a distribution of acid sites comparable to that of the *in situ* samples; however, for the SiZr (0.2-*ex*) and SiZr (0.25-*ex*) samples the proportion of Brønsted acidity was greatly decreased (Fig. 3 and Table 2, column 6), whereas the Lewis site density was significantly enhanced (Table 2, column 7) compared to the other

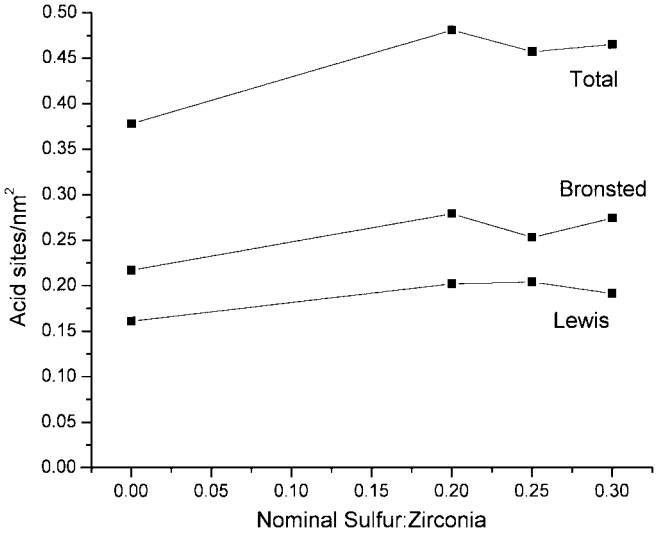

FIG. 2. Acid site distribution for *in situ* sulfated samples from pyridine retained after 423 K evacuation.

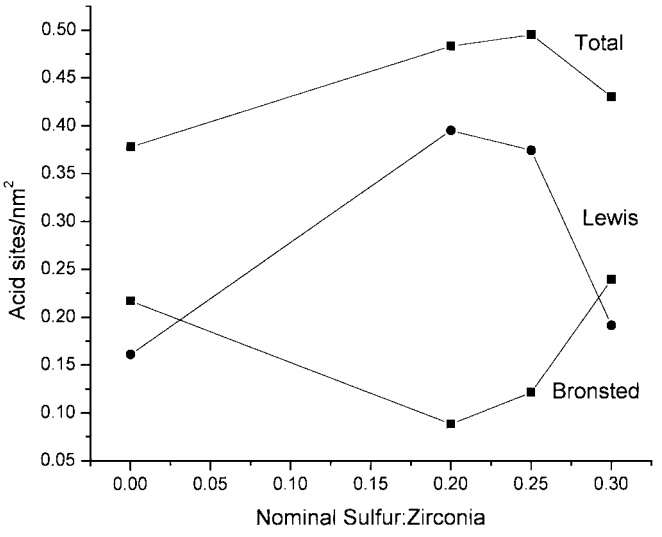

FIG. 3. Acid site distribution for *ex situ* sulfated samples from pyridine retained after 423 K evacuation.

mixed oxides. The ratio of n_{Lewis} (473 K)/n_{Lewis} (423 K) was used as an indicator of the relative strength of Lewis acid sites. Ratios were fairly consistent across the series of samples with all values lying in a narrow range between 0.68 and 0.72. The nonsulfated sample gave the highest of these ratios (0.72), indicating that Lewis acid strength was not enhanced by the process of sulfation.

XPS results (Table 3) show surface atomic ratios (columns 2 and 3) as well as the binding energies (obtained from deconvoluted peak maxima) for zirconium, oxygen, silicon, and sulfur. The most striking difference between the mixed oxides was the variation in the Si/Zr ratio from 2.3 for SiZr (0.3-*in*) to 3.81 for the segregated sample. There were also significant differences observed when the method of sulfation was varied; for example, the SiZr (0.3-*in*) gave a Si/Zr ratio of 2.3 compared to 3.48 for the SiZr (0.3-*ex*) sample, indicating major changes in surface composition following sulfation. The ratio of sulfur to zirconia also displayed significant changes between various samples, the most interesting being the difference between the SiZr (0.3-*ex*) sample with a S/Zr ratio of 0.2 compared with 0.15 for SiZr (0.25-*ex*). This difference is significant given that the elemental analysis showed the two samples to contain identical amounts of sulfur. The *in situ* sulfated samples show surface S : Zr ratios (Table 3) which increase in proportion with the amount of total retained sulfur (Table 1). The binding energies gave far less information with all mixed oxide samples giving similar results with no clear trend. The only exceptions were the appearance of a single zirconium species for the SiZr (0.25-*ex*) sample and a shift towards lower binding energies (BEs) observed for the segregated sample. Even the sulfated and nonsulfated zirconias gave identical profiles with no additional zirconium or oxygen species observed on sulfation.

TABLE 3

XPS Binding Energies and Surface Atomic Ratios

Sample	Si/Zr S/Zr	Zr $3d_{3/2}$ (eV)	Zr $3d_{5/2}$ (eV)	O 1*s* (eV)	Si 2*p* (eV)	S $2p_{1/2}$ (eV) S $2p_{3/2}$ (eV)
SiZr (0.30-*ex*)	3.48, 0.20	182.5, 183.3	184.8, 185.8	531.0, 532.5, 533.8	102.8, —	169.0, 170.3
SiZr (0.25-*ex*)	3.28, 0.15	182.9, —	185.1, —	531.1, 532.5, 533.6	102.8, —	169.3, 170.3
SiZr (0.3-*in*)	2.30, 0.20	182.7, 183.7	185.1, 186.1	531.0, 532.3, 533.4	102.4, 103.5	169.1, 170.2
SiZr (0.25-*in*)	2.30, 0.13	182.7, 183.8	185.1, 186.0	530.8, 532.3, 533.5	102.8, —	168.9, 170.0
SiZr (0.20-*in*)	2.36, 0.09	182.6, 183.7	185.0, 186.1	530.7, 532.2, 533.4	102.8, —	168.8, 169.7
SiZr (0)	2.63, —	182.6, 183.4	185.0, 185.8	531.0, 532.6, 533.9	102.8, —	—, —
Segregated	3.81, —	182, 182.8	184.3, 185.2	530.7, 532.3, 533.5	102.4, 103.5	—, —
ZrO_2	— —	182.5, —	184.9, —	530.6, 532.3, —	—, —	—, —
ZrO_2 (sulfated)	— 0.27	182.6, —	184.9, —	530.6, 532.4, —	—, —	169.2, 170.2

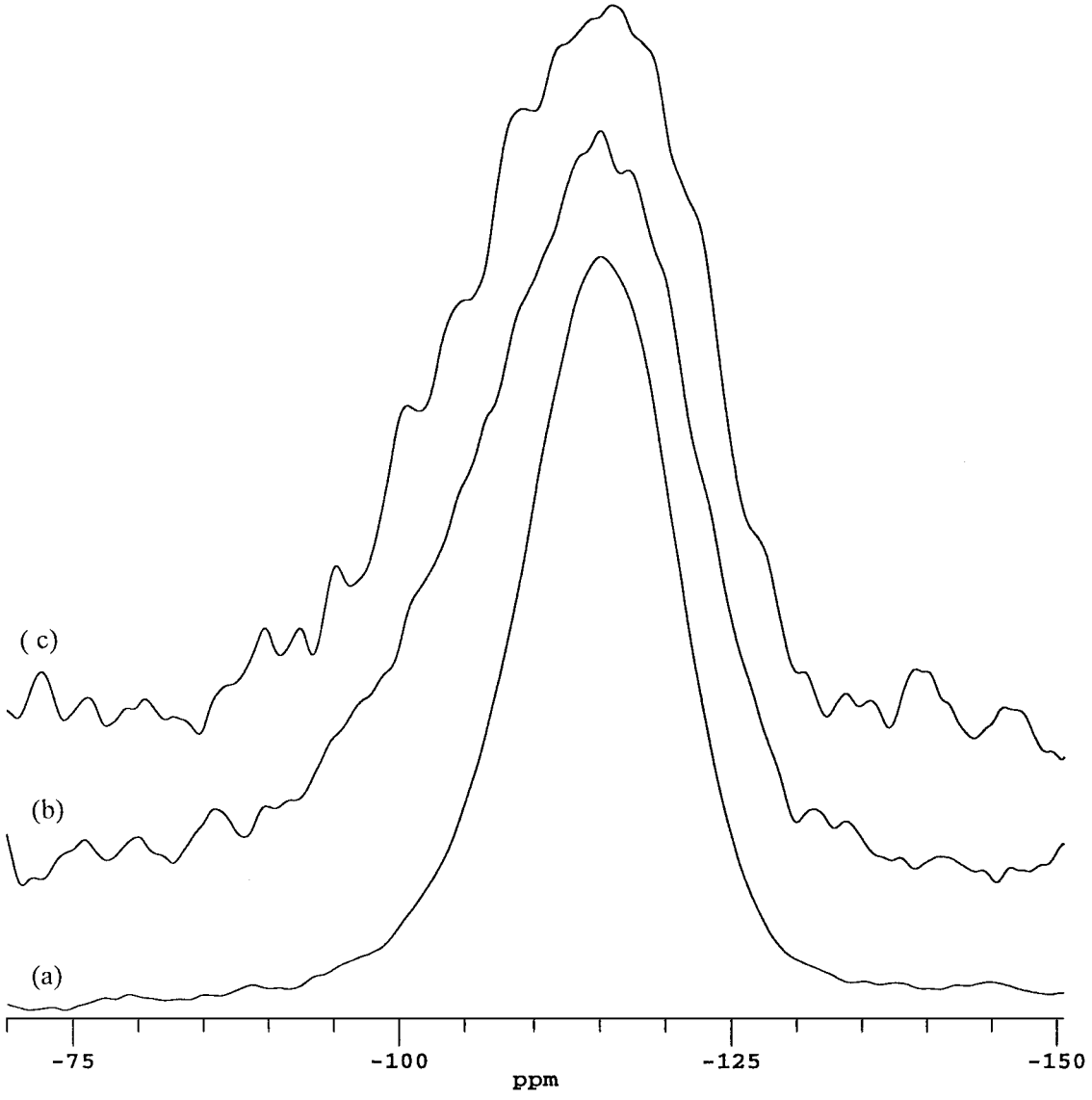

FIG. 4. ^{29}Si NMR spectra for (a) segregated, (b) representative sulfated (SiZr (0.3-*ex*)), and (c) nonsulfated samples recorded with a recovery time $\tau = 300$ s.

In addition to information provided by ^{29}Si T_1 relaxation times (Table 1) the shapes of the NMR signals resulting from the saturation recovery experiments can be of interest.^{29}Si spectra of amorphous silicas give broad features in the −90 to −120 ppm range (26) which result from contributions from Q^2, Q^3, and Q^4 silicon nuclei, where Q^x corresponds to a silicon nucleus with x siloxane linkages. The shape and linewidth of the spectra are expected (27) to show a strong dependency on the degree of crystallinity of the samples with more crystalline samples yielding sharper features. Spectra for the nonsulfated sample, a representative sulfated sample [SiZr (0.3-*ex*)], and the segregated samples are displayed in Fig. 4. All sulfated samples, whether prepared by *in situ* or *ex situ* methods, produced samples with similar ^{29}Si spectra. A narrowing of the overall peak envelope was observed as the relative contributions from different silica species changed when going from the nonsulfated to the segregated sample.

DISCUSSION

Nonsulfated Sample

Results for the current nonsulfated sample extend our work on the 33 mol% silica–zirconia sample (11) although a refined preparation procedure was adopted here. The objective of the work was to investigate modifications induced by sulfation, thus an extended discussion based on the differences arising from this modified procedure will not be given. However, to provide a starting point for discussion, some basic comparison details will be provided. The sulfate-free sample prepared using the current method, which involved higher solution dilution and extended prehydrolysis compared with a previous method (11), produced a higher surface area material (317 cf. 207 $m^2\,g^{-1}$) with significantly greater average pore diameter (20–60 cf. 3–4 nm). The higher area contained a reduced density of Lewis acid sites (0.161 cf. 0.305 nm^{-1}) but increased Brønsted acid density (0.217 cf. 0.137 nm^{-1}). The similarity (30.2 cf. 27.4 s) in spin-lattice relaxation times (T_1) would suggest (10) that the degree of mixing of the two oxide components was similar in both sample preparations. Further evidence (7) for the good degree of mixing was provided by X-ray diffraction, (XRD) which showed the sample to be amorphous after calcination at 873 K while tetragonal ZrO_2 was detected for silica-free sulfated zirconia heated at the same temperature. Silica-free zirconia samples are expected to crystallize between 773 and 873 K (28–31) with the addition of silica expected to delay this temperature; the greater the silica content, the greater this crystallization is suppressed (29, 31). DTA-TGA analysis of silica–zirconia mixed oxides indicates crystallization between 1050 and 1273 K (29, 31, 32) while XRD evidence for the formation of crystalline phases suggests temperatures between 973 and 1173 K (29, 31). Diffraction results here are consistent with literature reports (29, 31) that the expected crystalline phase obtained by calcination at 1373 K is cubic/tetragonal zirconia, although reports of transformations to monoclinic zirconia and $ZrSiO_4$ at 1473 K are known (31). The detection of zirconia-only phases requires that thermal treatment separate the phases leaving largely silica-only domains. The increase in T_1 from 30.2 to 96.4 (Table 1) would indicate (10) that all or the majority of the zirconia had migrated to the surface under these conditions. Pure silica and silica with zirconia deposited at the surface exhibit T_1 values for 110–117 s (10). Spin-lattice relaxation is, however, also affected by the proximity of Si nuclei to hydroxyl groups, and the sharpening of the ^{29}Si signal resulting from thermal treatment which leads to a symmetrical line at −115 ppm (Fig. 4, curve a) would suggest a largely hydroxyl-free system with Q^4 (siloxane units) dominating. The presence of signal between −100 and −110 ppm (Q^2 and Q^3 signals) for the nonsulfated sample prior to 1373 K treatment (Fig. 4, curve c) would be consistent with a higher degree of hydroxylation of this sample (33), although the difficulty in distinguishing between chemical shifts of $Si(–O–Si)_n$ $(–O–X)_{4-n}$ where X is H or Ti (34) or H or Zr (11) limits the extent of conclusions drawn from loss of signal in the −100 to −110 ppm region. It is clear that little more can be said than that thermal treatment at elevated temperature leads to a sharpening of the signal at −115 ppm with a system dominated by $Si(–O–Si)_4$ units as a result of elimination of the heterolinkages (either Si–O–H or Si–O–Zr). Part of the loss of heterolinkages results from segregation of the zirconia and migration to the surface as indicated by T_1 measurements and XRD analysis. The increase in Si/Zr ratio by XPS (2.63 to 3.81) following thermally induced sintering results from well-distributed surface zirconia forming sintered three-dimensional phases.

Acidity measurements should (7) reveal phase separation as well-mixed silica–zirconia show both Brønsted and Lewis acidity while the component oxides generate only the latter (in the case of ZrO_2) (7–11, 32, 35). However, it has been argued (11) that the presence of Brønsted acidity does not necessarily imply (7) a high degree of mixing throughout the bulk but rather indicates that a specific arrangement of units is made at a molecular level at the surface. That is, surface segregation of one component of a previously well mixed two-component oxide need not necessarily result in a lowering of the density of Brønsted acid sites. Brønsted acidity was enhanced (0.217 cf. 0.137 nm^{-1}) relative to our previously prepared sample (11) of the same SiO_2/ZrO_2 ratio. However, segregation of the phases by thermal treatment was accompanied by loss of surface area (Table 1), producing a solid which adsorbed less than 0.1 mg/g_{sample} and which consequently made impossible any analysis of numbers of types of acid site by FTIR. Breaking of heterolinkages to form well-defined segregated phases should produce notable changes in electron binding energies of the elements. Bosman *et al.* (36) found that the $Zr3d_{5/2}$ XPS peak appeared at ca. 1 eV higher for samples that were less

than 75% ZrO_2 in silica–zirconia mixed oxides. However, the peaks appear (before deconvolution) at 182.9 (nonsulfated) and 182.6 eV (segregated), suggesting that this parameter does not provide conclusive proof of heterolinkages prior to thermally induced phase separation. The O 1*s* signal was similarly unrevealing, showing maxima at 532.4 and 532.5 eV for the nonsulfated and segregated samples, respectively. The Si 2*p* signal showed only a 0.2-eV difference between the BE maxima, giving 102.7 eV for the phase segregated sample, somewhat lower than the 103.7 eV literature value for single oxide silica (36).

Ex Situ Sulfation

A nonsulfated sample which was subsequently treated with sulfuric acid solutions clearly led to textural changes in the mixed oxide, resulting in loss of pore volume and, consequently, BET surface area (Table 1). The increase in spin-lattice relaxation time from 30.2 to between 43.1 and 45.3 s (Table 1) would imply (10) that zirconia had been partially extracted from the bulk of the mixed oxide to leave larger domains containing silica alone, thus providing one reason for the structural changes. However, surface Si/Zr ratios of the sulfate-treated mixed oxides were higher (3.28 and 3.48) than the sample prior to sulfation (2.63). The two apparently conflicting facts can only be reconciled if extraction of zirconia to the surface is accompanied by agglomeration of zirconia to form small X-ray-amorphous particles. That is, acid treatment has a similar but less dramatic effect as the thermal treatment in that both induce surface segregation of zirconia to form a particulate zirconia phase. It was previously argued (11) that the generation of surface acid groups depends on the surface arrangement of the two component oxides rather than being related (7) to the degree of heterolinkage formation throughout the structure, so ignoring for the moment the influence of retained sulfate groups on acidity (30–32, 37–39), the extraction of zirconia to the surface and the formation of three-dimensional zirconia phases from the two-dimensional mixed surface layer of the mixed oxide should lead to significant modification of the acid sites present. Note that the Turin group (37, 39) has suggested that the use of a strong base such as pyridine may overestimate Lewis acidity on sulfated zirconia due to competition between the sulfate and the pyridine for the cationic centers. However, the removal of all weakly held sulfate by the high calcinations temperature used here (873 K, 6 h) prior to determination of the acid site density should ensure (39) that the data obtained using our procedure give an accurate determination of acid site densities. Lewis acid density in nonsulfated silica–zirconia aerogels shows a monotonic increase with mol% zirconia (11), so extraction of zirconia to the surface by sulfation would be expected to enhance the number of these centers. This is confirmed in Fig. 3 and Table 2 where SiZr (0.2-*ex*) and SiZr (0.25-*ex*) show Lewis acid densities that are ca. 2.5 times greater than the parent sulfate-free mixed oxide. This increased Lewis acid density as zirconia is extracted from the bulk is obtained despite a decrease in the surface Zr/Si ratio (Table 3) of 0.38 : 1 to 0.3 : 1 resulting from sulfation. This can only be rationalized if Lewis sites are formed only in silica-free zirconia regions rather than at exposed zirconia sites in well-mixed regions of the surface. The latter are more likely to be the source of Brønsted acid sites, leading to the prediction that loss of Brønsted acidity by phase separation in the surface layers would lead to enhanced Lewis acidity and vice versa. This is qualitatively consistent with the symmetrically shaped plots shown in Fig. 3, where loss of one type of acid site is matched by gain in the other. Similar effects have recently been obtained using phosphoric acid (40).

Unlike the changes in Brønsted and Lewis acid site densities induced by changing surface composition of silica–zirconia by a change in molar ratios (11), changes in acid site densities induced here by inorganic acid treatment may additionally result from acidity induced by retention of sulfate-type species. Samples SiZr (0.25-*ex*) and SiZr (0.3-*ex*) retain (Table 1) identical amounts of sulfur yet display (Fig. 3) widely different acid type and densities, which might invoke a preliminary conclusion that the amount of retained sulfur (sulfate) plays a minor role in acid site generation and that the nature of the treatment and the final surface composition of the component oxides is of greater importance. Although the measured sulfur concentration is identical for SiZr (0.25-*ex*) and SiZr (0.3-*ex*), the surface sulfur/Zr ratio is lower for the former (Table 3). This results from the higher surface Zr concentration for SiZr (0.25-*ex*) than SiZr (0.3-*ex*). (Note that direct comparison of surface ratios is possible here due to the almost identical (212 and 208 $m^2\ g^{-1}$) surface areas for these two samples.) The greater Zr/Si ratio for SiZr (0.25-*ex*) than SiZr (0.3-*ex*) would be expected (11) to generate a surface with a greater Lewis acid density for the former, which is consistent with the findings (Table 2 and Fig. 3). Maintaining the density of surface sulfur (sulfate), but increasing the S/Zr ratio as a result of reduced surface Zr for SiZr (0.3-*ex*) leads to a loss in Lewis acid sites as these become covered by sulfate species, which may themselves be the source of proton acidity (30–32, 37–39). The lower surface Zr levels for SiZr (0.3-*ex*) detected by XPS (Table 3) are most likely the consequence of larger three-dimensional amorphous clusters rather than reduced levels of extracted Zr from the bulk mixed oxide.

Assuming the 1.84 wt% sulfur (Table 1) measured by elemental analysis for SiZr (0.3-*ex*) is present as surface sulfate, then the density corresponds to 1.66 SO_4^{2-}/nm^2. However, should this sulfate be exclusively located on the zirconia component (21), then from the Si/Zr surface atomic ratio of 3.48 : 1 and using the values of 20.0 (41) and 8.1 $Å^2$ (42) for the unit areas occupied by ZrO_2 and SiO_2, respectively, the density of sulfate groups becomes 3.01 per nm^2 (exposed zirconia) for SiZr (0.3-*ex*). In the case of SiZr

(0.25-*ex*), this value is 2.82 SO_4^{2-}/nm^2(exposed zirconia). These densities are greater than the literature value of 2.5 groups per nm^2 that can be stabilized on silica-free zirconia (43), although the XPS S/Zr ratios are actually lower than for the sulfated ziconia (Table 3). If the density of acid sites (Table 2) is calculated per unit area of exposed zirconia, then the number of Brønsted sites/nm^2 becomes 0.21 for SiZr (0.25-*ex*) and 0.43 for SiZr (0.3-*ex*), which corresponds to an increase of 0.22 sites/nm^2 as a consequence of increasing the sulfate density by 0.19 SO_4^{2-}/nm^2 (exposed zirconia). That is, in this range of sulfate loadings, each additional sulfate creates about one Brønsted acid site. At the same time, the corresponding Lewis site densities (calculated per unit area of exposed zirconia) falls from 0.648 for SiZr (0.25-*ex*) to 0.347/nm^2, or 0.301 sites per nm^2 are lost as the sulfate loading increases by 0.19/nm^2.That is, each additional sulfate leads to the loss of 1.5 Lewis sites. This increase from 2.82 to 3.01 SO_4^{2-}/nm^2 (exposed zirconia) may correspond to the concentrations required to convert isolated sulfate species to disulfate (14) or polynuclear sulfates (44). This transition in the nature of sulfate species has been shown to increase the ratio of Brønsted sites to Lewis sites for sulfated zirconia (44). As each added sulfate leads to the formation of an additional Brønsted acid site under these conditions, it is clear that in this range of sulfate densities, these species are not merely "spectator" sulfate groups which may occur on sulfate-doped zirconia (45). At these levels of sulfate it should be noted that the total acid site density developed is only marginally greater than for the nonsulfated mixed oxide (Fig. 3), although the strength of the acid sites for the sulfated material is significantly greater (40). Note that Brønsted acidity is developed even though the highest S/Zr ratio is only 0.2 : 1, i.e., the amorphous phase is not zirconium sulfate but sulfate-coated oxide. These sulfates must be reasonably uniform as indicated by the sulfur XPS analysis, and the infrared band at ca. 1380 cm^{-1} would confirm that they contain at least one S=O bond. Further discussion of the role of sulfate follows the discussion of *in situ* preparation; however, to summarize, *ex situ* treatment of the silica–zirconia mixed oxide initially leads to enhanced numbers of Lewis acid sites at the expense of Brønsted sites, mainly as a result of induced zirconia segregation and loss of the Si–Zr mixing at the surface, whereas at higher sulfate concentrations, Brønsted acidity is created at the expense of Lewis sites when the surface sulfate concentration is greater than ca. 2.82 SO_4^{2-}/nm^2.

In Situ Sulfation

The use of sulfuric acid as hydrolysis catalyst allowed sulfate to be incorporated into the silica–zirconia mixed oxide during the preparation stages rather than as a postpreparation treatment. The textural nature of the resultant mixed oxide was quite dissimilar to the nonsulfated sample (Fig. 1) and the *ex situ* prepared samples (Table 1). Consistent with studies of sulfated zirconia aerogels using H_2SO_4 as hydrolysis catalyst (38), samples here retained a greater proportion of sulfur (sulfate) when applied during the preparation stage than when applied as a postpreparation treatment. Although bulk sulfate may migrate to the oxide surface especially during crystallization (38), it is most likely that part of the total sulfur is retained within the bulk of the material and is thus not directly implicated in the formation of acid sites at the surface of the mixed oxide. From the foregoing discussion for the *ex situ* prepared samples, one might expect that the amount of sulfate retained at the surface may be linked to the amount of amorphous zirconia (and, to a lesser extent, Zr–O–Si hetero linkage sites) at the surface, which in turn would depend on the acid concentration in solution following the condensation step; that is, some aging in solution might be expected, which would extract zirconia to the surface. However, although the sulfuric acid concentration is modified, the total acid concentration remained constant and thus the extent of extraction of zirconia during aging should be constant for the samples. This is confirmed by the similarity in Si/Zr surface ratios obtained by XPS for all of the *in situ* series (Table 3). Even allowing for the difference in surface areas, the Si/Zr surface atomic ratios for the nonsulfated and *in situ* sulfated samples are much closer than those for the *ex situ* treated samples, indicating that postpreparation treatment with sulfuric acid has a much greater influence on the extent to which zirconia segregation occurs. Although the XPS ratios reflect both the extent of extraction of zirconia from the bulk and the degree to which three-dimensional particle formation of this surface zirconia occurs, the shorter T_1 values for the *in situ* prepared samples (ca. 41 s) compared with the *ex situ* samples (ca. 44 s) would suggest (10) that zirconia extraction occurred to a lesser extent for the former. T_1 was still, however, longer for the *in situ* sulfated preparations than the nonsulfated sample, suggesting that poorer mixing, possibly resulting from some degree of segregation, does occur for the former. Confirmation that the amount of exposed zirconia in amorphous layers at the surface was less than for the *ex situ* treated samples was provided by the Lewis acid densities (Figs. 2, and 3), which are lower for the samples of nominal S/Zr < 0.3, and not substantially higher than in the nonsulfated sample (Table 2).

The amount of exposed, amorphous zirconia is thus expected to remain constant across the series of *in situ* sulfated samples, and a proportion of the total exposed zirconia which contributes to the high Zr/Si ratios determined by XPS may result from zirconia held within the silica–zirconia network. On the other hand, as sulfate is distributed between the bulk and the surface for the *in situ* series, an increase within the series from 1.54 to 3.00% S (Table 1) should result in increased levels of surface sulfate. XPS atomic ratios confirmed that the S/Zr surface ratio (Table 3) increases in proportion with the total amount of retained

sulfur (Table 1). However, the development of acid sites as a function of sulfate loading by the *in situ* samples is quite dissimilar to the tendency shown by *ex situ* prepared samples with no loss in Brønsted sites as Lewis sites are generated (and vice versa) and, instead, both types of site are present at densities which appear independent of the nominal (or retained) sulfur levels, although in all cases, these densities are marginally greater than in the nonsulfated material. Brønsted acid strengths were greater than in the nonsulfated material (40). It could be argued that the "crucial" sulfate loading of >2.82 SO_4^{2-}/nm^2 (exposed zirconia) was already achieved, even at 1.54% S. However, even if all of this sulfate were located at the surface, this would only equate to 1.32 SO_4^{2-}/nm^2 (total surface) or ca. 1.78 SO_4^{2-}/nm^2 (exposed ZrO_2).

To account for these data it is possible that lower sulfate densities are required to populate the zirconia surface of the *in situ* prepared samples due to the different morphology presented, although at these lower densities, the strong Brønsted acid sites detected (40) can still be generated. It is not difficult to imagine the surface zirconia on the *in situ* prepared samples to be quite dissimilar to that of the *ex situ* samples. Morterra *et al.* (44) have shown how the morphology of the surface zirconia is crucial in generating Brønsted acid sites on sulfate-doped zirconia. Additionally, the relative proportion of amorphous zirconia is expected to be low for the *in situ* preparation and so the majority of the zirconia detected by XPS remains in the mixed oxide network and adsorbs little or no sulfate. As the concentration of the amorphous zirconia phase is expected to be less than for the *ex situ* samples, relatively lesser amounts of adsorbed sulfate would be required to generate an equivalent number of the strong acid sites detected (40) that can only be generated for the *ex situ* sample at the highest sulfate loading. The critical sulfate loading may therefore be reached at relatively low levels of overall sulfation for the *in situ* samples because it is high in localized parts of the surface. In support of this argument, the absorption coefficients for the pyridinium ion, ε_{1540}, for the *in situ* samples stay fairly constant across the series, indicative of the similar localized environment, whereas only at SiZr (0.3-*ex*) does the ε_{1540} value fall within this range for the *ex situ* samples. Note that at this highest load for samples of each series, the surface S/Zr ratios concur (S/Zr = 0.2) and both samples exhibit similar Brønsted acid densities (Table 2).

The additional surface sulfate achieved by increasing the bulk sulfate loading apparently converts existing weaker Brønsted sites to stronger sites, as evidenced by the increased butene conversion activity for the sulfated samples relative to the nonsulfated material (40), although the total number of sites does not increase (Fig. 2). Note that for both series at the highest sulfate loading, the S/Zr ratio obtained by XPS reaches 0.20 : 1 for both samples, which is still below the value (0.27) for the sulfated zirconia (Table 3) again indicating that the nature of the exposed zirconia is paramount in dictating the maximum sulfate density which can be achieved.

The fact that densities of Brønsted (ca. 0.26/nm^2) and Lewis (ca. 0.20/nm^2) acid sites remain constant for the *in situ* samples as the overall nominal and measured sulfate concentrations increase would confirm that variation in the extent to which sites are generated for the *ex situ* samples occurs in the first instance due to variation in the amounts of amorphous zirconia extracted (which then influences the amount of retained sulfate).

CONCLUSIONS

Postpreparation treatment of amorphous silica–zirconia mixed oxide by sulfuric acid leads to a loss of surface area as a proportion of zirconia is extracted from the bulk and deposited as an amorphous oxide layer at the external surface. This extraction enhances Lewis acid density at the expense of Brønsted acidity. Sulfate is retained by the sample as an adsorbed species rather than as zirconium sulfate and when the surface density of sulfate groups is greater than ca. 2.82/nm^2 of exposed zirconia, Brønsted acidity is developed at the expense of Lewis acidity. This crucial level is reached at lower sulfate concentrations for the *in situ* prepared samples as less exposed amorphous zirconia is present, which, additionally, is probably morphologically distinct from the zirconia present in the *ex situ* prepared samples.

ACKNOWLEDGMENTS

We thank the University of Dundee for a University Studentship (D.J.R.) and Dr. R. W. McCabe and Mr. P. D. Cookson of the University of Central Lancashire for performing DTA analysis of the samples.

REFERENCES

1. Corma, A., *Chem. Rev.* **95**, 559 (1995).
2. Tanabe, K., Sumiyoshi, T., Shibata, K., Kiyoura, T., and Kitagawa, J., *Bull. Chem. Soc. Jpn* **47**, 1064 (1974).
3. Thomas, C. L., *Ind. Eng. Chem.* **41**, 2564 (1949).
4. Kataoka, T., and Dumesic, J. A., *J. Catal.* **112**, 66 (1988).
5. Liu, Z., Tabora, J., and Davis, R., *J. Catal.* **149**, 117 (1994).
6. Kung, H. H., *J. Solid State Chem.* **52**, 191 (1984).
7. Miller, J. B., and Ko, E. I., *Catal. Today* **35**, 269 (1997).
8. Miller, J. B., Rankin, S. E., and Ko, E. I., *J. Catal.* **148**, 673 (1994).
9. Anderson, J. A., and Fergusson, C. A., *J. Non-Cryst. Solids* **246**, 177 (1999).
10. Anderson, J. A., and Fergusson, C. A., *J. Mater. Sci. Lett.* **18**, 1075 (1999).
11. Anderson, J. A., Fergusson, C. A., Rodríguez-Ramos, I., and Guerrero-Ruiz, A., *J. Catal.* **192**, 344 (2000).
12. Morterra, C., Cerrato, G., Emanuel, C., and Boris, V., *J. Catal.* **142**, 349 (1993).
13. Morterra, C., Cerrato, G., Pinna, F., and Signoretto, M., *J. Phys. Chem.* **98**, 12373 (1994).
14. Clearfield, A., Serrette, G. P. D., and Khazi-Syed, A. H., *Catal. Today* **20**, 295 (1994).
15. Moreno, J. A., and Poncelet, G., *Appl. Catal., A* **210**, 151 (2001).

16. Hua, W., Goeppert, A., and Sommer, J., *J. Catal.* **197**, 406 (2001).
17. Jung, S. M., Dupont, O., and Grange, P., *Appl. Catal., A*. **208**, 393 (2001).
18. Barthos, R., Lónyi, F., Engelhardt, J., and Valyon, J., *Top. Catal.* **10**, 79 (2000).
19. Lopez, T., Tzompantzi, F., Navarrete, J., Gomez, R., Boldú, J. L., Muñoz, E., and Novaro, O., *J. Catal.* **181**, 285 (1999).
20. Miller, J. B., and Ko, E. I., *Chem. Eng. J.* **64**, 273 (1996).
21. Morrow, B. A., McFarlane, R. A., Lion, M., and Lavalley, J. C., *J. Catal.* **158**, 116 (1996).
22. Yoldas, B. E., *J. Non-Cryst. Solids* **38**, 81 (1980).
23. Mountjoy, G., Pickup, D. M., Anderson, R., Wallidge, G. W., Holland, M. A., Newport, R. J., and Smith, M. E., *Phys. Chem. Chem. Phys.* **2**, 2455 (2000).
24. Anderson, J. A., and Fergusson, C. A., unpublished results, 1998.
25. Flego, C., Kiricsi, I., Perego, C., and Bellussi, G., *Catal. Lett.* **35**, 125 (1995).
26. Mailer, L., Devreux, F., Chaput, F., Boilot, J. P., and Axelos, M. A. V., *J. Non-Cryst. Solids* **147/148**, 686 (1992).
27. Engelhard, G., and Michel, D., *in* "High Resolution Solid State NMR of Silicates and Zeolites," p. 195. Wiley, Chichester, 1987.
28. Tret'yakov, N. E., Pozdnyakov, D. V., Orkanskaya, O. M., and Filimanov, V. N., *Russ. J. Phys. Chem.* **44**, 596 (1970).
29. Navío, J. A., Marchena, F. J., Macías, M., Colón, G., Avilés, M. A., and Sánchez-Soto, P. J., *J. Sol.-Gel Sci. Technol.* **10**, 165 (1997).
30. Lónyi, F., Valyon, J., Engelhardt, J., and Mizukami, F., *J. Catal.* **160**, 279 (1996).
31. Aguilar, D. H., Torres-Gonzalez, L. C., Torres-Martinez, L. M., Lopez, T., and Quintana, P., *J. Solid State Chem.* **158**, 349 (2000).
32. Navío, J. A., Colón, G., Macías, M., Camplelo, J. M., Romero, A. A., and Marinas, J. M., *J. Mol. Catal.* **135**, 155 (1998).
33. Humbert, B., *J. Non-Cryst. Solids* **191**, 29 (1995).
34. Walther, K. L., Wokaun, A., Handy, B. E., and Baiker, A., *J. Non-Cryst. Solids* **134**, 47 (1991).
35. Barthos, R., Lónyi, F., Engelhardt, J., and Valyon, J., *Top. Catal.* **10**, 79 (2000).
36. Bosman, H. J. M., Pijpers, A. P., and Jaspers, A. W. M. A., *J. Catal.* **161**, 551 (1996).
37. Morterra, C., Cerrato, G., Pinna, F., and Meligrana, G., *Top. Catal.* **15**, 53 (2001).
38. Signoretto, M., Pinna, F., Strukul, G., Cerrato, G., and Morterra, C., *Catal. Lett.* **36**, 129 (1996).
39. Morterra, C., and Cerrato, G., *Phys. Chem. Chem. Phys.* **1**, 2825 (1999).
40. Rosenberg, D. J., and Anderson, J. A., unpublished results, 2002.
41. Márquez-Alvarez, C., Fierro, J. L. G., Guerrero-Ruiz, A., and Rodríguez-Ramos, I., *J. Colloid Interface Sci.* **159**, 454 (1993).
42. Chudek, J. A., Hunter, G., McQuire, G. W., Rochester, C. H., and Smith, T. F. S., *J. Chem. Soc., Faraday Trans.* **92**, 453 (1996).
43. Sarzanini, C., Sacchero, G., Pinna, F., Signoretto, M., Cerrato, G., and Mortera, C., *J. Mater. Chem.* **5**, 353 (1995).
44. Morterra, C., Cerrato, G., and Bolis., V., *Catal. Today.* **17**, 505 (1993).
45. Benaïssa, M., Santiesteban, J. G., Díaz, G., Chang, C. D., and José-Yacamán, M., *J. Catal.* **161**, 694 (1996).